Check for updates

A Generalized Model for Compliant Passive Bipedal Walking: Sensitivity Analysis and Implications on Bionic Leg Design

Aikaterini Smyrli
Department of Mechanical Engineering,
National Technical University of Athens,
9 Heroon Polytechniou Street,
Athens 15780, Greece
e-mail: katerinasmyrli@mail.ntua.gr

Georgios A. Bertos
Department of Mechanical Engineering,
National Technical University of Athens,
9 Heroon Polytechniou Street,
Athens 15780, Greece
e-mail: gbertos@central.ntua.gr

Evangelos Papadopoulos[1]
Fellow ASME
Department of Mechanical Engineering,
National Technical University of Athens,
9 Heroon Polytechniou Street,
Athens 15780, Greece
e-mail: egpapado@central.ntua.gr

The passive behavior of a compliant biped walking model, subject to variations in its design, is investigated. A biped gait model is developed that allows for studying the effects of leg impedance, geometry, foot curvature, and inertial properties on the stable gait performed passively. A set of nondimensional parameters has been produced that fully defines the compass gait behavior, eliminating the dependence of our results on scale. Models emerging from parameter combinations were tested on their ability to perform stable passive walking on slope, and the characteristics of the gait performed in each case were recorded. Investigation of parameter ranges allowed us to draw relationships between various gait characteristics and specific, nondimensional parameter selections. By mapping the changes in system behavior under simple design variations, this work facilitates the selection of design parameters at an early stage of designing bionic walking equipment, including prostheses and exoskeletons. [DOI: 10.1115/1.4051232]

1 Introduction

The study of bipedal locomotion has been a key point of interest during the past decades. To accompany clinical research performed on human subjects, a number of mechanical biped models describing walking dynamics have been produced to date, all of which resemble human lower limb anatomy, and simplify the complex task of analyzing human gait mechanics.

Clinical research has focused on quantifying the effect of parameter variations in human walking. Parameters such as the type of walking surface [1], the weight distribution [2,3], and subject health [4] have been studied to draw cause-and-effect relationships between them and gait characteristics. Various studies have drawn parallels between results from clinical trials and simple walking models [5–7].

Simple dynamics models have greatly assisted the study of human gait from a theoretical standpoint. Mochon and McMahon showcased the passive nature of the swing phase of walking for a biped model with knees [8]. McGeer first introduced the notion of passive walking (i.e., without any actuation), which is achievable by some bipedal machines, and conducted a detailed study on their gait characteristics [9]. Passive bipedal walking was soon linked to energetically efficient human walking, suggesting that the human lower limb structure facilitates this mode of locomotion due to its passive dynamics [10].

A number of different models have been employed for the study of gait mechanics. Garcia et al. introduced a simple double pendulum model of massless, rigid legs [11] that has been widely used in many subsequent studies for its simplicity [10,12]. McGeer's bipeds incorporated rigid legs, hip friction, and foot curvature [9]: his papers have inspired and influenced many future works [13], but the effects of compliance and therefore the double stance phase of walking were not studied. Alexander first introduced leg compliance to a simple biped model [14], which enabled a unification of walking and running biomechanics models [15,16] but did not study the effects of foot curvature on the gait produced. Gard et al. developed a rigid-leg, rocker-based, inverted pendulum model for the prediction of hip movement during human walking [17]. Kuo studied the lateral hip motion and resulting gait stability with a three-dimensional model of passive walking [18]. These studies have greatly contributed to the advancement of bipeds' understanding and allow us to match dynamic behaviors with the presence of abstract mechanical elements. However, elements can often work with or against one another, and their combination must also be studied for its dynamic behavior. As the biped's dynamics are nonlinear and include phase shifts, knowledge of the simpler models' dynamic behavior does not suffice to extract results for their combination in a single model, as the superposition principle is not valid for this type of systems: a unifying biped model is needed for this purpose.

Based on the present models, there have been some notable studies on the investigation of model parameter values with respect to gait characteristics. McGeer first studied the effect of parameter variations on his models [9]. Asano et al. studied the effect of foot curvature on walking speed and stability [19], as well as on energy dissipation [20]. They have proposed that semicircular feet profiles act as actuated joints, enabling the forward advancement of the biped [19]. Our team has also performed studies on the effects of various foot shapes in passive walking robots [21,22]. Van der Linde studied the effect of active leg compliance on hip trajectory for a passive walker with round feet [23]. Bertos et al. employed sinusoidal analysis [7] to identify the vertical mechanical impedance of the human locomotor [24], enhancing Gard's model with elastic and damping elements.

Parameter investigations have been conducted for other types of locomotion machines. Mombaur performed parameter optimization for open-loop stability in an actuated full-body model of human running [25]. Cherouvim et al. studied the effect of parameter variations in the hopping motion of a monopod [26]. Chatzakos et al. studied how the bounding motion of a quadruped robot is affected by parameter selection [27]. Myrisiotis et al. linked quadruped design parameters to locomotion patterns [28].

Recent interest in bionic gait-assisting equipment such as active prostheses and exoskeletal devices has driven researchers to investigate human–device interaction schemes. In these works, the energetic cost is the most common evaluation parameter

[1]Corresponding author.

Manuscript received January 16, 2021; final manuscript received May 14, 2021; published online June 17, 2021. Assoc. Editor: Francesco Travascio.

 Copyright © 2021 by ASME

Downloaded from http://asmedigitalcollection.asme.org/biomechanical/article-pdf/143/10/101008/6713527/bio_143_10_101008.pdf by National Technical University of Athens user on 18 June 2021

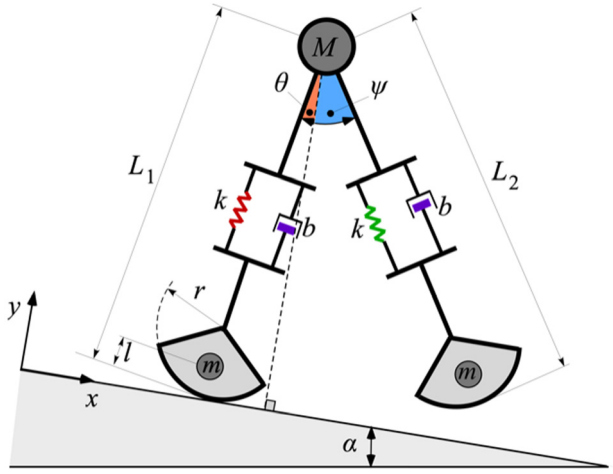

Fig. 1 The biped model during the single stance phase

[29,30], followed by trajectory tracking [31], locomotion speed, gait stability, and muscle fatigue [32]. Preliminary results on the passive behavior of the proposed biped model have been presented in Ref. [33]; that study focused on actively controlling a biped robot toward an efficient gait on level ground but did not investigate passive behavior thoroughly, apart from the biped's stability.

In this work, the passive gait performed on a negative slope by a biped model with compliant legs on semicircular feet is investigated. The biped's legs incorporate inertial elements. The mechanical losses are due to the axial leg dampers, as well as due to the impacts with the ground. To the best of our knowledge, no passive walking model simultaneously incorporating all these elements has been studied to date. This type of model allows us to determine the effects of design options, such as leg impedance, leg and foot geometric design, and mass distribution, and of their interactions, on the passive gait of the biped. A set of nondimensional parameters that describe the biped design—and consequently govern the gait characteristics—is identified, and a relationship between model scale-independent parameter selection and intrinsic gait characteristics such as passive stability, step frequency, speed, hip displacement and loading, and energetic efficiency is provided. Our intention is to develop a gait model that will provide assistance in the design of efficient bionic prostheses, exoskeletal devices, and biologically inspired walking robots. We believe that the proposed model's generalized design provides detailed and reliable results, and that the presented dimensional analysis approach will ease the implementation of our findings in real-world applications.

2 Methods

To investigate the effects of design choices in the characteristics of passive walking achieved by biped machines, a detailed model of the biped's passive dynamics is constructed first.

2.1 Model Structure and Parameters. The model studied (Fig. 1) is a rocker-based double-pendulum biped that performs passive walking in the x-direction of the x-y plane defined in Fig. 1. The biped is composed of deformable legs of uncompressed length L_{nat} that contain axial elastic and damping elements.

A key design parameter in this study is the legs' axial impedance. Elastic legs allow for smoother hip movements, modeling the compliance that knees normally introduce. The elastic degrees-of-freedom allow the inclusion of the walking double stance phase, where both legs are in contact with the ground. Damping elements along these elastic legs are responsible for energy losses during the biped's gait as well as for the subsequent decay in the legs' axial oscillations. We define the impedance constants of elasticity and damping as k and b, respectively. Varying values of k and b have been associated with changes in walking patterns [24].

The rockers used as the biped's feet simulate the rocking motion of the heel, ankle and forefoot complex [17,33]. Here, we assume semicircular, nondeformable feet of radius r that perform rolling without slipping on the ground.

The model's inertial properties are mainly due to the hip point mass M, which is fixed at the hip joint. Swing leg dynamics heavily depend on the foot point mass m. There are two such point masses in our biped, each fixed to one of the biped's feet, at a distance l from the foot bottom, see Fig. 1.

2.2 Foot-to-Ground Contact. To describe the motion of the biped mathematically, a set of assumptions is made, defining the foot-to-ground contact: (i) the contact is inelastic, and the contact surfaces are noncompliant, (ii) during the contact periods, the feet perform rolling without slipping, and (iii) any contact of the swing foot with the ground during its forward motion is ignored. Assumption (i) is possible due to the elasticity of the legs, and (ii) is confirmed by the simulation results by calculating the contact's friction coefficient. The latter assumption (iii) is due to the lack of knees that would allow the swing leg to clear the floor. However, this can be bypassed in the design of a physical prototype easily [9], without significantly affecting the passive dynamics, in which we are interested here.

Because of the model's plane formulation, (iv) we do not distinguish between a left and a right foot. For the leg angle variables to increase during each step, (v) θ and ψ are defined in opposite directions.

2.3 Walking Phases and Events. Walking is characterized by two distinct phases: the *single stance phase* (SSP) and the *double stance phase* (DSP). During the SSP, the stance leg supports the biped, while the swing leg advances forward.

The SSP ends with a *heel strike* (HS), when the swing leg touches the ground. The HS event initializes the DSP, where both legs are in contact with the ground. The DSP ends when the trailing leg leaves the ground during the *toe-off* (TO) event, initializing the next step's swing phase.

As can be observed from Fig. 1, in the SSP, the model has four degrees-of-freedom (DOFs). These are the two leg angles, defined with respect to the ground normal, θ for the stance leg, and ψ for the swing leg, and the two leg length variables, L_1 and L_2, respectively. The generalized variable vector $\mathbf{q}$ fully describes the biped's configuration

$$\mathbf{q} = [\theta, L_1, \psi, L_2]^T \tag{1}$$

whereas the state vector $\mathbf{x}$, which includes both the elements of $\mathbf{q}$ and their speeds $\dot{\mathbf{q}}$, describes the state of the model

$$\mathbf{x} = [\theta, \dot{\theta}, L_1, \dot{L}_1, \psi, \dot{\psi}, L_2, \dot{L}_2]^T \tag{2}$$

The biped's dynamic behavior during SSP is governed by a set of four nonlinear second-degree equations of motion: two of which govern the stance leg, while the other two determine the swing (contralateral) leg dynamics. The dynamics can be derived in matrix form as

$$\mathbf{M}(\mathbf{q})\ddot{\mathbf{q}} + \mathbf{C}(\mathbf{q}, \dot{\mathbf{q}})\dot{\mathbf{q}} + \mathbf{K}(\mathbf{q}) + \mathbf{G}(\mathbf{q}) = \mathbf{0} \tag{3}$$

where $\mathbf{M}_{4\times4}$ is the system inertia matrix; $\mathbf{C}_{4\times4}$ is a matrix due to centrifugal, Coriolis, and damping terms; $\mathbf{K}_{4\times1}$ is the stiffness vector; and $\mathbf{G}_{4\times1}$ is the gravity vector. Their elements are given in the Appendix.

As there are no inputs in the right-hand side of Eq. (3), the SSP equations of motion for the n^{th} step are solved for their response

Downloaded from http://asmedigitalcollection.asme.org/biomechanical/article-pdf/143/10/101008/6713527/bio_143_10_101008.pdf by National Technical University of Athens user on 18 June 2021

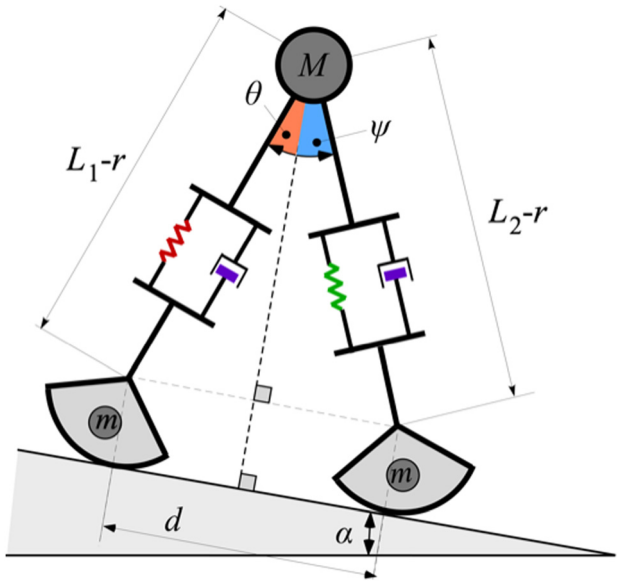

Fig. 2 The model during the double stance phase

to the initial step conditions $\mathbf{x}_n$. The SSP ends at HS of the swing leg, where the state vector $\mathbf{x}_{n,HS}$ is appointed as initial conditions to the next phase of walking.

During the DSP, model assumptions (i) and (ii), i.e., inelastic contact and rolling without slipping, define two separate geometric constraints that must be met by the model, also see Fig. 2. Using the subscript HS to denote variable values at HS, these two constraints are expressed as

$$s_1(\mathbf{q}) = (L_1 - r)\cos\theta - (L_2 - r)\cos\psi = 0 \tag{4}$$

$$s_2(\mathbf{q}) = d_{HS} - d + r(\theta_{HS} - \theta + \psi_{HS} - \psi) = 0 \tag{5}$$

where d is the distance between the two semicircular feet's geometric centers, as shown in Fig. 2, and is defined in Eq. (6)

$$d = (L_1 - r)\sin\theta + (L_2 - r)\sin\psi \tag{6}$$

To satisfy these constraints during DSP, Eq. (3) is extended with the addition of the generalized constraint force vector $\mathbf{f}_{4\times1}$ and Eqs. (4) and (5) are required to be satisfied by the system solutions, thus limiting the DOFs to only two. Then, the constraint-appended biped dynamics during the DSP are described by

$$\begin{aligned}\mathbf{M}(\mathbf{q})\ddot{\mathbf{q}} + \mathbf{C}(\mathbf{q},\dot{\mathbf{q}})\dot{\mathbf{q}} + \mathbf{K}(\mathbf{q}) + \mathbf{G}(\mathbf{q}) - \mathbf{f} &= \mathbf{0}\\ \mathbf{s}(\mathbf{q}) &= \mathbf{0}\end{aligned} \tag{7}$$

where $\mathbf{s}_{2\times1}=[s_1,s_2]^T$ is the constraint vector and the rest of the terms have been defined in Eq. (3).

The generalized constraint force vector $\mathbf{f}$ is calculated via the multiplication of the constraint matrix $\mathbf{\Pi}_{2\times4}$ with the Lagrange multiplier vectors λ_1 and λ_2, corresponding to constraints s_1 and s_2, respectively, and composing the vector $\boldsymbol{\lambda}_{2\times1}$

$$\mathbf{f} = \mathbf{\Pi}^T(\mathbf{q})\boldsymbol{\lambda} \tag{8}$$

The elements of the constraint matrix $\mathbf{\Pi}$ are listed in the Appendix, and given by

$$\pi_{jk} = \frac{\partial s_j}{\partial q_k}, \quad j = 1\ldots2,\ k = 1\ldots4 \tag{9}$$

The dynamics of Eq. (7) are solved for their response to DSP's initial conditions $\mathbf{x}_{n,HS}$ when there exists a small relative velocity between the swing foot and the ground. At that instant, the constraint forces $\mathbf{f}$ decelerate the swing foot to conform its velocity with the constraints in $\mathbf{s} = \mathbf{0}$, resulting in a HS impact, see Fig. 3. The DSP dynamics are solved until the event TO, at which point the state vector is $\mathbf{x}_{n,TO}$.

The integration of the SSP dynamics (3) starts at the beginning of each step and ends at HS. According to assumption (iii), the event HS is defined so that any contact of the swing foot with the ground during the foot's forward advancement is ignored. To achieve this, three conditions must be met simultaneously

$$(L_1 - r)\cos\theta - (L_2 - r)\cos\psi = 0 \tag{10}$$

$$\psi > 0 \tag{11}$$

$$\frac{d}{dt}[(L_1 - r)\cos\theta - (L_2 - r)\cos\psi] < 0 \tag{12}$$

Conditions (10)–(12) are identified as the foot-on-ground condition, swing leg advancement condition, and swing leg retraction condition, respectively, Eq. (10) defines the stance foot's contact with the ground, Eq. (11) is satisfied when the swing leg has advanced forward of the hip joint, and Eq. (12) translates to the swing foot descending toward the ground. The termination of the DSP is defined to occur when the trailing leg foot mass weight is lifted from the ground, when the ground reaction force on the foot becomes zero.

2.4 Gait Function Definition. Up to this point, a single step of the biped model has been defined fully; still the gait dynamics must be expressed in a compact way. This will allow solving for repetitive gait cycles and determining the parameters that define gait dynamics.

We define as f_1 the dynamic process governed by the SSP dynamics (3) that maps the state vector $\mathbf{x}_n$ at the beginning of the nth step to the state vector $\mathbf{x}_{n,HS}$ at HS

$$\mathbf{x}_{n,HS} = f_1(\mathbf{x}_n) \tag{13}$$

Similarly, f_2 denotes the process of mapping the state vector $\mathbf{x}_{n,HS}$ at HS to the state vector $\mathbf{x}_{n,TO}$ at TO, through the integration of DSP dynamics (7)

$$\mathbf{x}_{n,TO} = f_2(\mathbf{x}_{n,HS}) = f_2(f_1(\mathbf{x}_n)) \tag{14}$$

Because of assumptions (iv) and (v), the elements of $\mathbf{x}_{n,TO}$ are transformed to obtain the initial state of the $(n+1)$th step

$$\begin{aligned}\theta_{n+1} &= -\psi_{n,TO},\ \psi_{n+1} = -\theta_{n,TO}\\ \dot{\theta}_{n+1} &= -\dot{\psi}_{n,TO},\ \dot{\psi}_{n+1} = -\dot{\theta}_{n,TO}\\ L_{1,n+1} &= L_{2,n,TO},\ L_{2,n+1} = L_{1,n,TO}\\ \dot{L}_{1,n+1} &= \dot{L}_{2,n,TO},\ \dot{L}_{2,n+1} = \dot{L}_{1,n,TO}\end{aligned} \tag{15}$$

The variables on the left-hand side of Eq. (15) are the elements of the initial condition state vector $\mathbf{x}_{n+1}$. Using Eq. (15), this transformation can be written in matrix form as

$$\mathbf{x}_{n+1} = \mathbf{T}\mathbf{x}_{n,TO} \tag{16}$$

where $\mathbf{T}_{8\times8}$ is a transformation matrix, whose sole nonzero elements are $t_{15} = t_{26} = t_{51} = t_{62} = -1$, $t_{37} = t_{48} = t_{73} = t_{84} = 1$.

Combining Eqs. (14) and (16) results in expressing the initial conditions of the $(n+1)$th step as a function of the initial conditions of the nth step. We call this *gait function* $\mathbf{p}$

$$\mathbf{x}_{n+1} = \mathbf{T}f_2(f_1(\mathbf{x}_n)) \triangleq \mathbf{p}(\mathbf{x}_n) \tag{17}$$

2.5 Model-Defining Parameters. Expressing each stage of Eq. (17) in nondimensional form allows for isolation of a set of six nondimensional parameters that fully define $\mathbf{p}$. To derive the dimensionless model, the L_{nat}, M and the acceleration of gravity,

Downloaded from http://asmedigitalcollection.asme.org/biomechanical/article-pdf/143/10/101008/6713527/bio_143_10_101008.pdf by National Technical University of Athens user on 18 June 2021

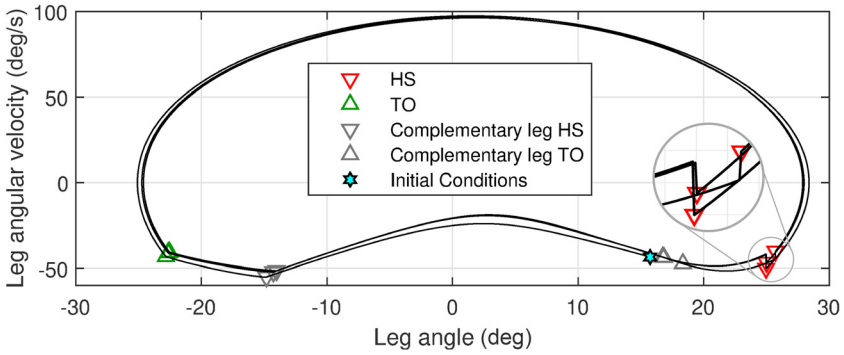

Fig. 3 Convergence to stable gait for 10 steps, demonstrates fixed point stability. The chart should be read in a clockwise direction. Initial conditions, HS and TO events are marked in the graph. Initial conditions are outside the fixed-point phase plot. Note the velocity spike due to the impact at HS, and the curvature change after the HS and TO events of both legs.

g, are selected as the characteristic parameters for length, mass, and acceleration, respectively. The resulting nondimensional model-defining parameters are the slope angle α, the damping parameter β, the elasticity parameter κ, the foot mass distribution parameter λ, the foot-to-hip mass ratio μ, and the rolling factor ρ. The analytical expression for these parameters can be found in Table 1.

Different parameter combinations lead to different gait functions. Therefore, we select a range of values for each parameter and focus on values that correspond to physically achievable models that are passively stable due to their design. This value range for each of the six parameters has been empirically selected to enclose the region of optimally stable designs, and is presented in Table 1, as well.

2.6 Repetitive Passive Gait and Fixed Points. To study passive walking, it is essential to identify repetitive passive gaits performed by the biped and to assess its ability to sustain them in the case of small perturbations.

Following Eq. (17), to identify states that can lead to passive walking, Eq. (18) must be solved for $\mathbf{x}$

$$\mathbf{x} = \mathbf{p}(\mathbf{x}) \tag{18}$$

Because of the nonlinearity of the problem, no analytical solution can be derived. Instead, a Newton–Raphson numerical method is employed $k+1$ times

$$\mathbf{x}_n^{\langle k+1\rangle} = \mathbf{x}_n^{\langle k\rangle} + (\mathbf{I}_{8\mathrm{x}8} - \nabla\mathbf{p}(\mathbf{x}_n^{\langle k\rangle}))^{-1}[\mathbf{p}(\mathbf{x}_n^{\langle k\rangle}) - \mathbf{x}_n^{\langle k\rangle}] \tag{19}$$

which is solved repetitively until convergence, using the following termination criterion:

$$\max_i \left| \frac{x_{i,\mathrm{n}}{}^{\langle k+1\rangle} - x_{i,\mathrm{n}}{}^{\langle k\rangle}}{x_{i,\mathrm{n}}{}^{\langle k\rangle}} \right| < 10^{-6} \tag{20}$$

Table 1 Nondimensional model parameters

Parameter, name	Definition	Minimum value	Nominal value	Maximum value
α, slope angle	α	−3.5 deg	−2 deg	0 deg
β, damping parameter	$b\sqrt{L_{\mathrm{nat}}}/(M\sqrt{g})$	0	3.5	5
κ, elasticity parameter	$kL_{\mathrm{nat}}/(Mg)$	10	29.7	70
λ, foot mass distribution	l/L_{nat}	0	0.15	1
μ, hip-to-foot mass ratio	m/M	0.001	0.02	0.1
ρ, rolling factor	r/L_{nat}	0	0.25	0.8

where x_i is the ith element of $\mathbf{x}$. The state vector $\mathbf{x}^*$ resulting from this process satisfies (18) and is called a *fixed point* of $\mathbf{p}$. It corresponds to states that, following a full cycle, return to themselves.

As has been discussed previously, different combinations of nonlinear model parameters (see Table 1) result in different gait functions $\mathbf{p}$, which in turn have different fixed points. Here, we attempt to make an optimal selection for our model's parameters, in terms of gait stability.

Fixed points $\mathbf{x}^*$ can be assessed regarding their stability, through the linearization of $\mathbf{p}$ around $\mathbf{x}^*$

$$\Delta\mathbf{x}_{\mathrm{n+1}}^* = \left.\frac{\partial\mathbf{p}(\mathbf{x}^*)}{\partial\mathbf{x}}\right|_{\mathbf{x}=\mathbf{x}^*} \Delta\mathbf{x}_{\mathrm{n}}^* \triangleq \mathbf{A}\Delta\mathbf{x}_{\mathrm{n}}^* \tag{21}$$

In Eq. (21), $\Delta\mathbf{x}^* = \mathbf{x} - \mathbf{x}^*$ is a small deviation of the state vector from its fixed point value. The eigenvalues of $\mathbf{A}_{8\times8}$ determine the stability of the discrete, linearized system (21): if all eigenvalues have a magnitude less than 1, then the linearized system and the fixed point $\mathbf{x}^*$ are considered to be stable.

It is important to note that due to the use of a linear stability criterion for a nonlinear system, the characterization of a fixed point as per its stability might be subject to inaccuracies. For this reason, every fixed point that has been found by Eq. (19) and characterized as stable using the linearized evaluation method described above is also tested for its ability to converge stably toward its fixed point, starting from initial conditions outside the fixed-point trajectory, see Fig. 3.

3 Results

3.1 Nominal Biped Model for Optimal Stability. System stability was evaluated for different parameter combinations starting from a reasonable set where the existence of a stable passive gait was found, and a *nominal* parameter set, resulting in an optimally stable gait, was numerically found via a cyclic coordinate descent optimization algorithm. The maximum eigenvalue magnitude, $|e|_{\max}$, of $\mathbf{A}$ resulting from parameter sweeps is presented in Fig. 4, where each point corresponds to results obtained when one of the parameters is altered from its nominal value. Nominal parameter values have been marked in the same plot by an inverted triangle (∇). The sweeping range for each parameter has been defined in Table 1. The effectiveness of the optimization process is evident in Fig. 4, as nominal values correspond to a minimum in $|e|_{\max}$. This optimal set defines the *nominal biped*; its parameters are given in Table 1.

As can be seen in Fig. 4, the range of values that lead to a stable gait differs qualitatively amongst the six parameters. The graphs corresponding to parameters α and β present a basin of stable gaits

Downloaded from http://asmedigitalcollection.asme.org/biomechanical/article-pdf/143/10/101008/6713527/bio_143_10_101008.pdf by National Technical University of Athens user on 18 June 2021

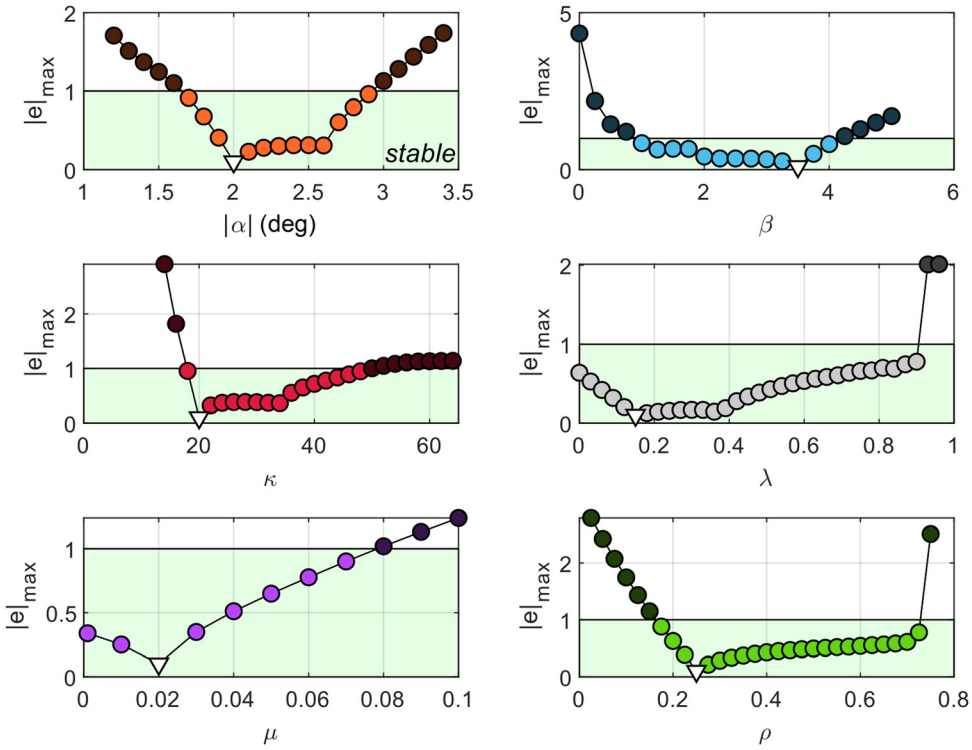

Fig. 4 Gait stability, sensitivity to nondimensional model parameters. For stability, $|e|_{max} < 1$. Nominal design is marked with a white triangle. Biped design variations are investigated for their stability by changing the value one parameter at a time from its nominal value.

around their corresponding minima, while values that lay further away from the nominal points are unstable. This is a result of the energetic equilibrium of stable gaits: as evidenced by the dynamic Eqs. (3) and (7), the energetic input depends on α while the energetic output on β; these must be matched to equate power input and loss and maintain the kinetic energy level of the system.

Intermediate values of κ and ρ facilitate step-to-step transitions by introducing compliance in the DSP. Very small values of κ lead to very compliant legs that are unable to support the biped's weight. On the other hand, very large values of κ introduce extreme rigidity and lead to asymptotically unstable gaits. Similarly, very small values of ρ do not facilitate rollover, while for values of ρ close to 1, the biped converges toward a rolling disk accelerating down a slope. Finally, μ and λ also present basin-type, complementary stability diagrams, implying that there exists an optimal weight distribution that presents optimal gait stability.

Comparing the stability range among the model's parameters leads to the observation that the system is not uniformly sensitive to variations of its nondimensional parameters. Specifically, the mass ratio μ and mass distribution λ present a narrow stability range, indicating that the swing leg pendulum dynamics heavily influence the biped's ability to perform passive gaits. On the other hand, the elasticity parameter κ presents a wide range of stable values, which is attributed to the system's gradual convergence to a stiff-legged walker as κ increases.

Moreover, we can draw positive results concerning the robustness of the passive gait, as the system appears to be stable for small parameter variations from the nominal point, along all six parameters. This observation is very important for our nominal model selection since our goal is to study passive gait characteristics for a broad range of parameter values, which introduces the need for stability robustness.

To demonstrate the stability of the nominal gait, Fig. 3 presents the phase space of the nominal biped, initiating gait with initial conditions outside its fixed-point trajectory. It can be observed that, after two steps, the passive gait converges to the trajectory corresponding to its stable fixed point.

3.2 Effect of Parameter Variations. To better study the behavior of the biped model and to link gait characteristics to model parameters, the gait performed by bipeds whose dimensionless parameters vary from the nominal set by a single parameter each time is studied. Here, gaits are evaluated based on their step frequency, hip vertical displacement, forward walking speed, hip accelerations, and energetic consumption. In the following plots, larger circles correspond to larger values for the investigated parameter. To allow model verification and investigate design suitability, the results presented correspond to human-compatible values of leg length $L_{nat} = 1$ m and hip mass $M = 80$ kg.

Subject to its passive dynamics, the biped tends toward performing steps at a specific frequency. Since there is no external input, this frequency must be determined by model parameters. To this end, an investigation was performed to identify the system parameters that affect step frequency.

Figure 5 provides a graphic interpretation of step frequency, by plotting simulation results on axes of step length, S_l, versus mean velocity in the x-direction, v_x. According to the laws of dimensional analysis and simple physics, step frequency is obtained as the ratio of v_x over S_l; this indicates that gaits with the same frequency yield pairs (S_l, v_x) that lie on a single line that intersects the origin. While this is true for most of the simulations plotted in Fig. 5, gaits that result from variations of parameters α, κ, and λ appear to have different step frequencies. Points that lay under the shaded region of Fig. 5 correspond to gaits that have a lower step frequency, whereas the opposite holds for points plotted above it.

In more detail, the slope angle α shapes the geometry of the biped's surroundings, affecting the frequency of HS events, and defines the effect of gravity, which has the biggest impact on passive walking. Smaller slope angles fail to accelerate the biped forward and result in smaller step frequencies. While increasing the value of α (larger circles) initially increases step frequency; once a certain value is reached, further increasing α has no effect on the frequency's value. This is because even though gravity increasingly facilitates forward advancement, HS occurs later in the step cycle.

Downloaded from http://asmedigitalcollection.asme.org/biomechanical/article-pdf/143/10/101008/6713527/bio_143_10_101008.pdf by National Technical University of Athens user on 18 June 2021

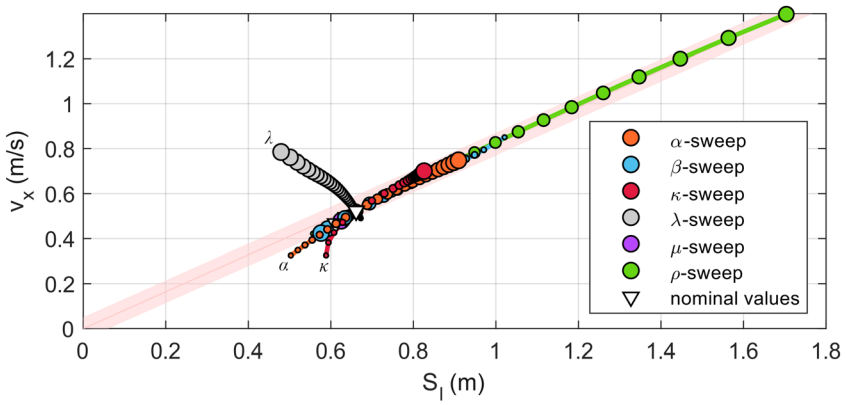

Fig. 5 Step frequency as the ratio of gait velocity over step length. Most points lie around a single line of constant frequency $f \approx 0.8$ Hz; points corresponding to variations of λ, α, and κ present a notable exception.

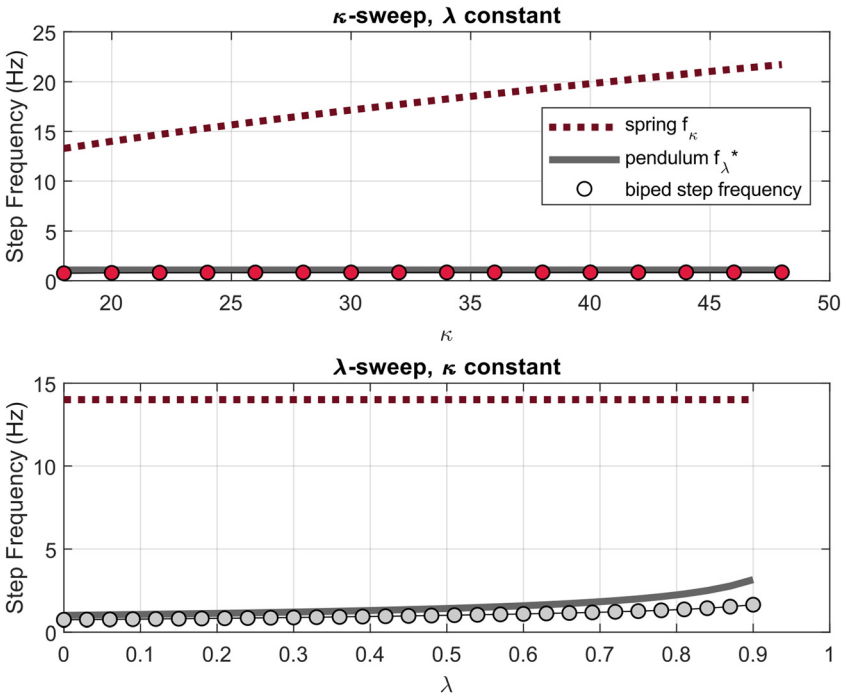

Fig. 6 Model simulated step frequency in comparison to resonance frequencies of elastic legs f_κ and swing leg pendulum motion, f_λ^*. Gait step frequency remains close to pendulum-related f_λ^*.

Our model is composed of two discrete subsystems: the pendula and the mass-spring-dampers. The effect of each of these on the step frequency of the biped is analyzed below.

We denote the subsystem frequency component that depends on parameter p by f_p. Elasticity parameter κ defines the resonance frequency f_κ of the model elastic legs, while foot mass distribution parameter λ defines the swing leg's pendulum resonance frequency f_λ. Using the parameter expressions of Table 1, we can observe from Eqs. (22) and (23) that f_κ and f_λ increase with κ and λ, respectively,

$$f_\kappa = \sqrt{\frac{k}{M}} = \sqrt{\frac{\kappa g}{L_{\text{nat}}}} \tag{22}$$

$$f_\lambda = \frac{1}{2\pi}\sqrt{\frac{g}{L_{\text{nat}} - l}} = \frac{1}{2\pi}\sqrt{\frac{g}{L_{\text{nat}}(1-\lambda)}} \tag{23}$$

Swing leg dynamics evolve over half the period of a free pendulum, ending at HS; we thus expect to observe double the frequency calculated in Eq. (23), defined as f_λ^*

$$f_\lambda^* = 2f_\lambda \tag{24}$$

To determine the effect of each subsystem's resonance frequencies on the step frequency of the biped, we plot the step frequency obtained by varying κ and λ from their nominal values, together with the plots of spring and pendulum natural frequencies calculated by Eqs. (22) and (24). Figure 6 presents this comparison. Step frequencies remain closer to f_λ^*, i.e., the pendulum frequency that primarily affects step dynamics. This points out that the leg compliance dynamics are secondary to the pendulum motion in determining step frequency. This can be explained by the fact that the step frequency depends on v_x and S_l, which are both associated with the pendulum motion.

The reason for our model's passive step frequency being smaller than its theoretical value calculated as f_λ^* as seen in Fig. 6

Downloaded from http://asmedigitalcollection.asme.org/biomechanical/article-pdf/143/10/101008/6713527/bio_143_10_101008.pdf by National Technical University of Athens user on 18 June 2021

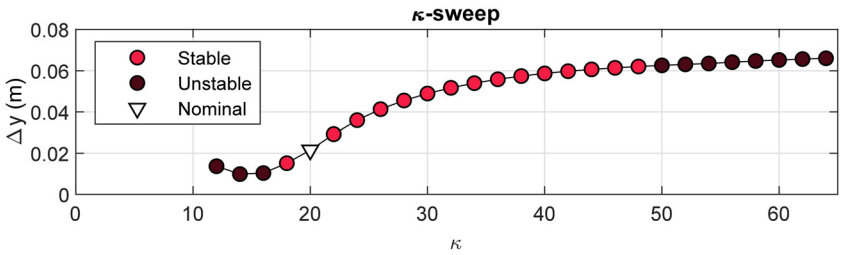

Fig. 7 Vertical hip displacement Δy for various leg elastic constants κ. Compliant legs allow for minimization of hip displacement.

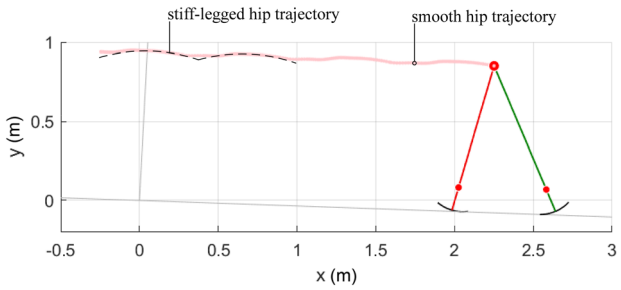

Fig. 8 Hip trajectory of our nominal biped during its stable fixed-point gait. The presence of elastic elements along the legs results in a smoother hip trajectory in comparison to a stiff-legged model, reducing the hip's inertial accelerations.

is that Eq. (23) is an approximation valid for small angular deviations of the pendulum from its equilibrium position (less than 4 deg). For larger angle values, as are observed in the steps of the biped, the resonance frequency of the pendulum motion decreases, resulting in smaller step frequencies.

Typical human walking step frequencies are in the range 1.4–2.5 Hz [34]. The passive pendulum dynamics lead to smaller step frequencies for a given velocity in our nonactuated model than is observed in human walking.

The vertical displacement of the hip Δy should be limited during walking, to minimize the displacement enforced on the human torso or on a robot's electronics. In humans, Δy values are in the range from 20 to 80 mm [17]. It is therefore interesting to study the effect of varying the elastic constant κ on the simulated value of this vertical displacement, Δy.

The displacement, Δy, is plotted in Fig. 7 for deviations of κ from its nominal value. This figure shows that the predicted displacements Δy are within the range of 20–80 mm, as noted earlier, with the smaller displacements occurring for low κ. Figure 7 also shows that for smaller κ values, the hip displacement is considerably lower than for stiffer legs. Therefore, a careful selection of κ can reduce Δy to 20 mm ($\kappa \approx 20$). This is an interesting design characteristic that can be used to minimize hip oscillatory movements without the need for active control. Very soft legs ($\kappa < 20$) fail to support the body and result in unstable passive gaits, while with very stiff legs, ($\kappa > 50$), the biped converges to a rigid-legged walking pattern.

The elastic elements introduced by κ affect not only the hip displacement but also its rate of change. Elastic legs of smaller κ enable the biped to achieve a smoother transition during the DSP, minimizing the accelerations acting on the hip. Figure 8 presents the trajectory achieved by the nominal biped's hip, comparing it to the hip trajectory of a biped with fully stiff legs. It is evident that the elastic legs smoothen the hip's trajectory, reducing its inertial accelerations.

Generally, the hip inertial acceleration in the y-direction is proportional to inertial loads applied at the hip. Consequently, we study the relationship between mean forward gait velocity v_x and hip RMS vertical accelerations a_y, with the goal of identifying parameter combinations that satisfy speed and loading criteria for a given application.

In Fig. 9, the procedure described in Section A was followed, this time plotting results on a velocity-acceleration plane (in Fig. 9, larger circles mark larger parameter values). A quick observation of the graph suggests that the values of velocity and acceleration are mostly proportional, with faster gaits often translating to larger hip inertial loads.

In general, both v_x and a_y increase when α, κ, and ρ take greater values, while larger β values lead to slower gait paces and smaller hip accelerations. This is due to the mass-spring-damper system, where RMS accelerations increase with spring rigidity, here

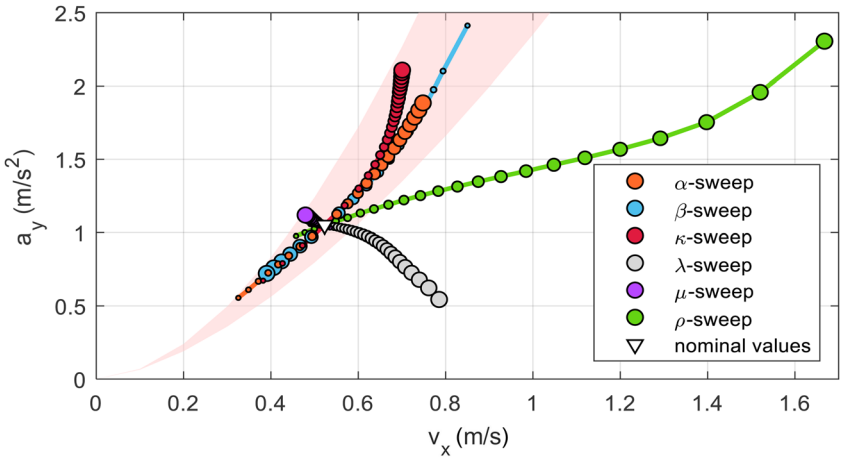

Fig. 9 Mean forward velocity plotted against hip RMS vertical acceleration for various parameter variations from nominal model. Inertia-related parameters can lead to smaller hip loads for large walking velocities.

Downloaded from http://asmedigitalcollection.asme.org/biomechanical/article-pdf/143/10/101008/6713527/bio_143_10_101008.pdf by National Technical University of Athens user on 18 June 2021

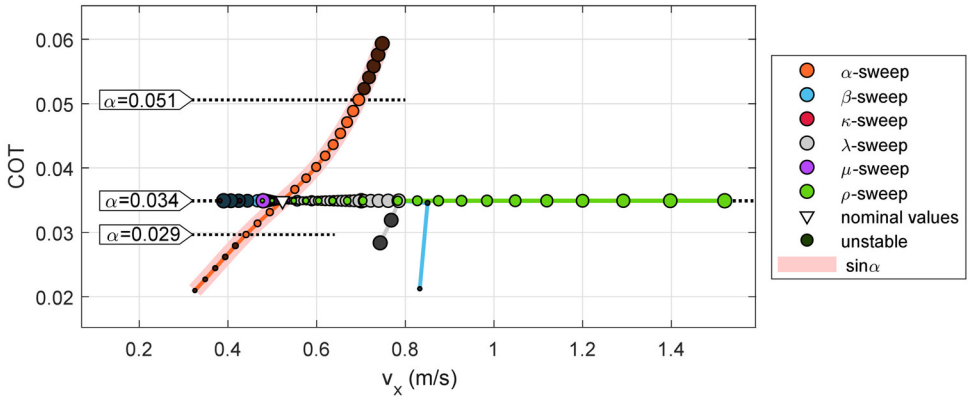

Fig. 10 COT only depends on slope α. Foot curvature-defining ρ leads to larger velocity for the same energy level, maintaining gait stability.

proportional to κ, and decrease with the damping constant, which is proportional to β. A further increase of κ with respect to its nominal value would result to a vertical asymptote in the diagram, implying infinitely large hip loads for a finite speed.

It is also expected that an increase in slope angle α will lead to a faster gait and that steeper descents cause greater inertial loads. The effect of increasing the rolling factor ρ is to increase the biped's forward velocity, introducing a small but increasing amount of hip loads in doing so. However, for a given forward velocity, gaits obtained by varying ρ achieve lower vertical accelerations than those resulting from varying α, κ, or β.

However, the effect of parameters μ and λ is significantly different: legs of larger moment of inertia, indicated by larger μ and smaller λ, result in larger impact during HS, and they are also slower to bring forward, due to their smaller f_λ^*, resulting in smaller forward gait velocity. The opposite holds for legs of smaller moment of inertia, of small μ and large λ.

Typical RMS values for the vertical hip acceleration during human walking are in the range 0.49–4.91 m/s^2 [35], again matching our model's predictions.

Faster locomotion is often associated with greater energy losses; however, this is not always the case in passive walking. Figure 10 presents the biped's cost of transport (COT) as a function of mean forward velocity v_x. The COT is

$$\mathrm{COT} = \frac{\bar{P}_{\mathrm{loss}}}{(M+2m)gv_x} \tag{25}$$

where $\bar{P}_{\mathrm{loss}}$ is the average power loss of the system, calculated as the sum of damping and ground impact losses: the latter are calculated as the change in kinetic energy just before and after the impact. It can be observed that COT values do not depend on forward velocity v_x, but instead they directly relate to the slope angle α. For stable passive gaits, the COT is equal exactly to sinα [9], while deviations occur for some unstable gaits; this relationship is plotted in Fig. 10. This equality is attributed to the conservation of system kinetic energy during a stable gait.

It can be observed from Fig. 10 that greater values of the rolling factor ρ lead to stable passive walking with larger walking velocities without any increase in the energetic expense required for the gait. Therefore, in this case, the biped achieves higher velocities without an increase in the associated losses. However, it should be taken into consideration that very large values of ρ might result in impractical designs. Figure 10 shows also that the rest of the model's parameter variations lead to unstable gaits for velocities smaller than those achieved through ρ and are therefore less efficient in increasing the biped's velocity while preserving gait stability.

The energy input in this study has been provided by the biped's descent in the gravity field: this is a simplified way to perform simulations without an active energy input. The gait produced can be replicated on level ground with a model-based actuation scheme, without a significant increase in COT [33]. In humans and bionic devices, the energy input is provided by actuated joints in the hip, knees, and ankles.

Human metabolic costs during walking are above 0.26 J N^{-1} m^{-1} [36]. However, note that this figure differs from COT as it includes various vital metabolic functions that our model does not account for. An estimate for the human COT is 0.03–0.08 [37], while bipedal robots have reported COT in the range 0.04–0.08 [38], both matching our model's predictions.

4 Discussion

Our investigation highlights the dependence of lower limb passive behavior on design choices that are usually made early during the first stages of any gait-assisting system development. We have established relations between leg design and walking stability, step frequency, speed, hip vertical displacement and loading, and energetic efficiency.

The results show that different sets of design parameters satisfy different criteria; to avoid conflicts, the application aims and the appropriate evaluation criterion must be selected early on. The process of selecting a design for optimized gait stability has been presented here (Fig. 4).

With a goal of achieving more frequent steps, it is required to position the legs' center of mass closer to the hip. The opposite holds if aiming at a lower frequency gait (Figs. 5 and 6). The elasticity of the legs also changes gait frequency, but to a smaller extent (Fig. 6).

Hip displacement, an important value indicating comfort in walking, can be minimized by fine-tuning leg elasticity. Very stiff leg designs do not benefit from the effects of compliance and lead to hip displacements identical to the ones observed in rigid leg designs. Instead, hip movement is smoothened by selecting a more compliant design, resulting in minimal hip displacement (Figs. 7 and 8).

Decreasing the legs' moment of inertia, i.e., moving the legs' center of mass closer to the hip, significantly reduces hip loading while also increasing gait velocity. For a given leg mass distribution, the presence of damping elements can decrease the load at the hip at the cost of decelerating the walker. The opposite holds for large values of leg stiffness. Faster gaits with a low level of hip loading can be achieved by increasing foot curvature (Fig. 9).

An increased foot curvature also benefits leg designs by allowing larger gait velocities for a given energy consumption rate. In fact, it appears to be the only parameter able to result in high speeds without simultaneously compromising gait stability for a given COT (Fig. 10). This is very important in the design of prosthetic or exoskeletal devices, as the COT is a measure of the

Downloaded from http://asmedigitalcollection.asme.org/biomechanical/article-pdf/143/10/101008/6713527/bio_143_10_101008.pdf by National Technical University of Athens user on 18 June 2021

metabolic cost of walking: small COT allows for effortless movement. Variable-curvature foot designs, as is observed during human foot-rolling progression, might be a practical solution.

The biped studied here combines some key elements present in human walking in an abstract form, such as walking compliance, foot rollover, and leg inertia. However, it does not describe the detailed human design: there is no supporting torso or swinging arms, actuated knees, or ankles: all these have been shown to affect the dynamics and energetics of walking [39–41]. Despite its limitations, the biped's behavior has been found to highly resemble human walking characteristics, implying a high level of compatibility between assistive bionic devices dynamically resembling the presented design and human subjects.

More complex models would allow a more detailed comparison between the biped's dynamics and human gait. However, the abstract nature of this model includes the salient features of walking and allows for many design interpretations, to work around individual needs. To investigate the generalization capabilities of the abstract modeling approach, several passive biped variations can be studied and compared. For example, relocating the biped's damping elements at the hip joint, or substituting leg compliance with passive knee joints, would result in passive bipeds of similar structure, yielding results comparable to the ones obtained here.

In conclusion, the simulation and study of this model's passive dynamic behavior employing nondimensional parameters can help in a systematic, case-specific design investigation of gait-related questions, including lower limb prosthetic and orthotic devices' design options, at an early stage before manufacture and implementation. Our next plan is to build a walking machine to validate the proposed model and to develop and test bionic leg designs suitable for gait assistance based on the conclusions of this study.

5 Conclusion

This paper provides a design investigation of a biped model that can facilitate the understanding of efficient walking mechanisms in humans. We extracted this information by studying the characteristics of the biped's passive gait, when design parameters such as leg impedance, mass distribution, and foot curvature are altered. We obtained a set of design parameters that fully describe a nondimensional walking model. The focus of this work has been the study of the effect of parameter variations on the characteristics of the gait produced. We believe that a careful parameter selection can lead to an optimal design that will facilitate the efficient operation of gait-assisting bionic devices.

Nomenclature

$\mathbf{A}$ = matrix for the linearization of $\mathbf{p}$
a_y = rms vertical hip acceleration
b = axial leg damping
$\mathbf{C}$ = matrix for centrifugal, Coriolis, damping terms
COT = cost of transport of gait
d = distance between the two semicircular feet's geometric centers
DSP = double stance phase
$|e|_{\max}$ = maximum magnitude of $\mathbf{A}$'s eigenvalues
$\mathbf{f}$ = generalized constraint force vector
f_κ = resonance frequency of elastic legs
f_λ = resonance frequency of pendulum
f_λ^* = double the resonance frequency of pendulum
g = acceleration of gravity
$\mathbf{G}$ = gravity vector
HS = heel strike
k = axial leg elasticity constant
$\mathbf{K}$ = stiffness vector
l = distance of foot point mass from leg bottom
L_1 = stance foot leg length, generalized variable
L_2 = swing foot leg length, generalized variable
L_{nat} = uncompressed leg length
m = foot point mass
M = hip point mass
$\mathbf{M}$ = system inertia matrix
$\mathbf{p}$ = gait function
$\bar{P}_{\text{loss}}$ = average power loss of the system
$\mathbf{q}$ = generalized variable vector
r = circular foot radius
$\mathbf{s}$ = constraint vector during DSP
S_l = step length
SSP = single stance phase
$\mathbf{T}$ = end of step transformation matrix
TO = toe off
v_x = mean forward gait velocity
$\mathbf{x}$ = state vector
$\mathbf{x}^*$ = fixed point of $\mathbf{p}$
$\mathbf{x}_n$ = state at the beginning of n$^{\text{th}}$ step
$\mathbf{x}_{n,\text{HS}}$ = state at HS of nth step
$\mathbf{x}_{n,\text{TO}}$ = state at TO of nth step
α = slope angle
β = dimensionless damping parameter
Δy = maximum vertical displacement of the hip
θ = stance foot leg angle, generalized variable
κ = dimensionless elasticity parameter
λ = dimensionless foot mass distribution parameter
$\boldsymbol{\lambda}$ = Lagrange multiplier vector
μ = dimensionless hip to foot mass ratio
$\boldsymbol{\Pi}$ = constraint Jacobian
ρ = dimensionless rolling factor
ψ = swing foot leg angle, generalized variable

Appendix

The elements of the matrices $\mathbf{M}$, $\mathbf{C}$, $\mathbf{K}$, $\mathbf{G}$, and $\boldsymbol{\Pi}$ are

$$
\begin{aligned}
m_{11} &= M[(L_1-r)^2 + r^2 + 2r(L_1-r)\cos\theta] \\
&\quad + m\{(L_1-r)^2 + (L_1-l)^2 + 2r^2 \\
&\quad + 2r[(L_1-r)+(l-r)]\cos\theta\} \\
m_{12} &= m_{21} = (M+m)r\sin\theta \\
m_{13} &= m_{31} = m(L_2-l)[(L_1-r)\cos(\psi+\theta) + r\cos\psi] \\
m_{14} &= m_{41} = m[(L_1-r)\sin(\psi+\theta) + r\sin\psi] \\
m_{22} &= M+m,\ m_{23} = m_{32} = m(L_2-l)\sin(\psi+\theta) \\
m_{24} &= m_{42} = -m\cos(\psi+\theta),\ m_{33} = m(L_2-l)^2 \\
m_{34} &= m_{43} = 0,\ m_{44} = m
\end{aligned}
\tag{A1}
$$

$$
\begin{aligned}
c_{11} &= -\{[M(L_1-r) + m[(L_1-r)+(l-r)]r\sin\theta\}\dot{\theta} \\
c_{12} &= 2(M+m)(L_1-r+r\cos\theta)\dot{\theta} \\
c_{13} &= -m[(L_2-l)r\sin\psi + (L_1-r)(L_2-l)\sin(\psi+\theta)]\dot{\psi} \\
c_{14} &= 2m[(L_1-r)\cos(\psi+\theta) + r\cos\psi]\dot{\psi} \\
c_{21} &= -(M+m)(L_1-r)\dot{\theta},\ c_{22} = b \\
c_{23} &= m(L_2-l)\cos(\psi+\theta)\dot{\psi},\ c_{24} = 2m\sin(\psi+\theta)\dot{\psi} \\
c_{31} &= -m(L_1-r)(L_2-l)\sin(\psi+\theta)\dot{\theta} \\
c_{32} &= 2m(L_2-l)\cos(\psi+\theta)\dot{\theta},\ c_{33} = 0 \\
c_{34} &= 2m(L_2-l)\dot{\psi},\ c_{41} = m(L_1-r)\cos(\psi+\theta)\dot{\theta} \\
c_{42} &= 2m\sin(\psi+\theta)\dot{\theta},\ c_{43} = -m(L_2-l)\dot{\psi},\ c_{44} = B
\end{aligned}
\tag{A2}
$$

$$
k_1 = 0,\ k_2 = k(L_1 - L_{\text{nat}}),\ k_3 = 0,\ k_4 = k(L_2 - L_{\text{nat}}) \tag{A3}
$$

Downloaded from http://asmedigitalcollection.asme.org/biomechanical/article-pdf/143/10/101008/6713527/bio_143_10_101008.pdf by National Technical University of Athens user on 18 June 2021

$$
\begin{aligned}
g_1 &= g\{(M+m)[r\sin a + (L_1 - r)\sin(a-\theta)] \\
&\quad + m[r\sin a + (l-r)\sin(a-\theta)]\} \\
g_2 &= g(M+m)\cos(a-\theta) \\
g_3 &= gm(L_2 - l)\sin(a+\psi),\ g_4 = -gm\cos(a+\psi)
\end{aligned} \tag{A-4}
$$

$$
\begin{aligned}
&\pi_{11} = (L_1 - r)\sin\theta,\ \pi_{21} = r + (L_1 - r)\cos\theta \\
&\pi_{12} = -\cos\theta,\ \pi_{22} = \sin\theta,\ \pi_{13} = -(L_2 - r)\sin\psi \\
&\pi_{23} = r + (L_2 - r)\cos\psi,\ \pi_{14} = \cos\psi,\ \pi_{24} = \sin\psi
\end{aligned} \tag{A-5}
$$

References

[1] Menz, H. B., Lord, S. R., and Fitzpatrick, R. C., 2003, "Acceleration Patterns of the Head and Pelvis When Walking on Level and Irregular Surfaces," Gait Posture, **18**(1), pp. 35–46.

[2] Hansen, A. H., and Childress, D. S., 2005, "Effects of Adding Weight to the Torso on Roll-Over Characteristics of Walking," J. Rehabil. Res. Dev., **42**(3), pp. 381–390.

[3] Browning, R. C., Baker, E. A., Herron, J. A., and Kram, R., 2006, "Effects of Obesity and Sex on the Energetic Cost and Preferred Speed of Walking," J. Appl. Physiol., **100**(2), pp. 390–398.

[4] Iosa, M., Fusco, A., Morone, G., Pratesi, L., Coiro, P., Venturiero, V., De Angelis, D., Bragoni, M., and Paolucci, S., 2012, "Assessment of Upper-Body Dynamic Stability During Walking in Patients with Subacute Stroke," J. Rehabil. Res. Dev., **49**(3), pp. 439–450.

[5] Buczek, F. L., Cooney, K. M., Walker, M. R., Rainbow, M. J., Concha, M. C., and Sanders, J. O., 2006, "Performance of an Inverted Pendulum Model Directly Applied to Normal Human Gait," Clin. Biomech., **21**(3), pp. 288–296.

[6] Usherwood, J. R., Szymanek, K. L., and Daley, M. A., 2008, "Compass Gait Mechanics Account for Top Walking Speeds in Ducks and Humans," J. Exp. Biol., **211**(23): pp. 3744–3749.

[7] Bertos, G. A., Childress, D. S., and Gard, S. A., 2003, "A Steady State Sinusoidal Analysis Method to Identify the Mechanical Impedance of the Human Locomotor System During Able-Bodied Walking," 26th International Conference of Rehabilitation Engineering & Assistive Technology of North America (RESNA '03), Atlanta, GA, June 19–23, pp. 380–383.

[8] Mochon, S., and McMahon, T. A., 1980, "Ballistic Walking: An Improved Model," Math. Biosci., **52**(4-3): pp. 241–260.

[9] McGeer, T., 1990, "Passive Dynamic Walking," Int. J. Rob. Res., **9**(2): pp. 62–82.

[10] Kuo, A. D., 2002, "Energetics of Actively Powered Locomotion Using the Simplest Walking Model," ASME J. Biomech. Eng., **124**(1), pp. 113–120.

[11] Garcia, M., Chatterjee, A., Ruina, A., and Coleman, M. J., 1998, "The Simplest Walking Model: Stability, Complexity, and Scaling," ASME J. Biomech. Eng., **120**(2), pp. 281–288.

[12] Gregg, R. D., Dhaher, Y. Y., Degani, A., and Lynch, K. M., 2012, "On the Mechanics of Functional Asymmetry in Bipedal Walking," IEEE Trans. Biomed. Eng., **59**(5): pp. 1310–1318.

[13] Espiau, B., and Goswami, A., 1994, "Compass Gait Revisited," IFAC Symposium on Robot Control, Capri, Italy, Sept. 19–21, pp. 839–846.

[14] Alexander, R., 1992, "A Model of Bipedal Locomotion on Compliant Legs," Philos. Trans. R. Soc. London B Biol. Sci., **338**(1284), pp. 189–198.

[15] Owaki, D., Osuka, K., and Ishiguro, A., 2008, "On the Embodiment That Enables Passive Dynamic Bipedal Running," IEEE International Conference on Robotics and Automation (ICRA '08), Pasadena, CA, May 19–23, pp. 341–346.

[16] Geyer, H., Seyfarth, A., and Blickhan, R., 2006, "Compliant Leg Behaviour Explains Basic Dynamics of Walking and Running," Proc. R. Soc. London B Biol. Sci., **273**(1603), pp. 2861–2867.

[17] Gard, S. A., and Childress, D. S., 2001, "What Determines the Vertical Displacement of the Body During Normal Walking?," J. Prosthet. Orthotics, **13**(3), pp. 64–67.

[18] Kuo, A. D., 1999, "Stabilization of Lateral Motion in Passive Dynamic Walking," Int. J. Rob. Res., **18**(9), pp. 917–930.

[19] Asano, F., and Luo, Z. W., 2006, "On Energy-Efficient and High-Speed Dynamic Biped Locomotion with Semicircular Feet," IEEE/RSJ International Conference on Intelligent Robots and Systems (IROS '06), Beijing, China, Oct. 9–15, pp. 5901–5906.

[20] Asano, F., and Luo, Z. W., 2007, "The Effect of Semicircular Feet on Energy Dissipation by Heel-Strike in Dynamic Biped Locomotion," IEEE International Conference on Robotics and Automation (ICRA '07), Rome, Italy, Apr. 10–14, pp. 3976–3981.

[21] Smyrli, A., Ghiassi, M., Kecskeméthy, A., and Papadopoulos, E., 2019, "On the Effect of Semielliptical Foot Shape on the Energetic Efficiency of Passive Bipedal Gait," IEEE/RSJ International Conference on Intelligent Robots and Systems (IROS '19), Macau, China, Nov. 3–8, pp. 6302–6307.

[22] Smyrli, A., and Papadopoulos, E., 2020, "A Methodology for the Incorporation of Arbitrarily-Shaped Feet In Passive Bipedal Walking Dynamics," IEEE International Conference on Robotics and Automation (ICRA '20), Paris, France, May 31–Aug. 31, pp. 8719–8725.

[23] Linde, R. Q. V. D., 1998, "Active Leg Compliance for Passive Walking," IEEE International Conference on Robotics and Automation (ICRA '98), Leuven, Belgium, May 20, pp. 2339–2344.

[24] Bertos, G. A., Childress, D. S., and Gard, S. A., 2005, "The Vertical Mechanical Impedance of the Locomotor System During Human Walking with Applications in Rehabilitation," IEEE International Conference on Rehabilitation Robotics, (ICORR '05), Chicago, IL, June 28–July 1, pp. 380–383.

[25] Mombaur, K., 2009, "Using Optimization to Create Self-Stable Human-Like Running," Robotica, **27**(3), pp. 321–330.

[26] Cherouvim, N., and Papadopoulos, E., 2006, "Energy Saving Passive- Dynamic Gait for a One-Legged Hopping Robot," Robotica, **24**(4), pp. 491–498.

[27] Chatzakos, P., and Papadopoulos, E., 2007, "Parametric Analysis and Design Guidelines for a Quadruped Bounding Robot," Proceedings of 15th IEEE Mediterranean Conference on Control and Automation, Athens, Greece, June 27–29, pp. 1–6.

[28] Myrisiotis, D., Poulakakis, I., and Papadopoulos, E., 2015, "On the Effects of Design Parameters on Quadruped Robot Gaits," IEEE International Conference on Robotics and Biomimetics (ROBIO '15), Zhuhai, China, Dec. 6–9, pp. 1072–1077.

[29] Sawicki, G. S., and Khan, N. S., 2016, "A Simple Model to Estimate Plantarflexor Muscle–Tendon Mechanics and Energetics During Walking with Elastic Ankle Exoskeletons," IEEE Trans. Biomed. Eng., **63**(5), pp. 914–923.

[30] Gams, A., Petrič, T., Debevec, T., and Babič, J., 2013, "Effects of Robotic Knee Exoskeleton on Human Energy Expenditure," IEEE Trans. Biomed. Eng., **60**(6), pp. 1636–1644.

[31] Khademi, G., Mohammadi, H., Richter, H., and Simon, D., 2018, "Optimal Mixed Tracking/Impedance Control with Application to Transfemoral Prostheses with Energy Regeneration," IEEE Trans. Biomed. Eng., **65**(4), pp. 894–910.

[32] Dollar, A. M., and Herr, H., 2008, "Lower Extremity Exoskeletons and Active Orthoses: Challenges and State-of-the-Art," IEEE Trans. Rob., **24**(1): pp. 144–158.

[33] Smyrli, A., Bertos, G., and Papadopoulos, E., 2018, "Efficient Stabilization of Zero-Slope Walking for Bipedal Robots Following Their Passive Fixed-Point Trajectories," IEEE International Conference on Robotics and Automation (ICRA '18), Brisbane, Australia, May 21–25, pp. 5733–5738.

[34] Cavagna, G. A., and Franzetti, P., 1986, "The Determinants of the Step Frequency in Walking in Humans," J. Physiol., **373**(1), pp. 235–242.

[35] Perry, J., 1992, *Gait Analysis: Normal and Pathological Function*, SLACK, Thorofare, NJ.

[36] Weyand, P. G., Smith, B. R., Puyau, M. R., and Butte, N. F., 2010, "The Mass-Specific Energy Cost of Human Walking Is Set by Stature," J. Exp. Biol., **213**(23), pp. 3972–3979.

[37] Donelan, J. M., Kram, R., and Kuo, A. D., 2002, "Mechanical Work for Step-to-Step Transitions is a Major Determinant of the Metabolic Cost of Human Walking," J. Exp. Biol., **205**(23), pp. 3717–3727.

[38] Collins, S. H., and Ruina, A., 2005, "A Bipedal Walking Robot With Efficient and Human-Like Gait," Proceedings of the IEEE International Conference on Robotics and Automation (ICRA'05), Barcelona, Spain, Apr. 18–22, pp. 1983–1988.

[39] Collins, S. H., Adamczyk, P. G., and Kuo, A. D., 2009, "Dynamic Arm Swinging in Human Walking," Proc. R. Soc. B Biol. Sci., **276**(1673), pp. 3679–3688.

[40] Umberger, B. R., 2008, "Effects of Suppressing Arm Swing on Kinematics, Kinetics, and Energetics of Human Walking," J. Biomech., **41**(11), pp. 2575–2580.

[41] Kuo, A. D., Donelan, J. M., and Ruina, A., 2005, "Energetic Consequences of Walking Like an Inverted Pendulum: Step-to-Step Transitions," Exer. Sport Sci. Rev., **33**(2), pp. 88–97.

Downloaded from http://asmedigitalcollection.asme.org/biomechanical/article-pdf/143/10/101008/6713527/bio_143_10_101008.pdf by National Technical University of Athens user on 18 June 2021